 CMES, vol.71, no.1, pp.39-66, 2011

Stochastic Meshless Local Petrov-Galerkin (MLPG) Method for Thermo-Elastic Wave Propagation Analysis in Functionally Graded Thick Hollow Cylinders

Seyed Mahmoud Hosseini[1], **Farzad Shahabian**[2]
Jan Sladek[3] **and Vladimir Sladek**[3]

Abstract: The thermo-elastic wave propagation based on Green-Naghdi (GN) coupled thermo-elasticity (without energy dissipation) is studied in a functionally graded thick hollow cylinder considering uncertainty in constitutive mechanical properties under thermal shock loading. The meshless local Petrov-Galerkin method accompanied with Monte-Carlo simulation is developed to solve the stochastic boundary value problem. In the presented method, the mechanical properties of FGM are considered to be as random variables with Gaussian distribution and mean values equal to deterministic values reported in previous works, which are generated using Monte-Carlo simulation with various coefficients of variations (COVs). The time evolution for transient problems is treated by using the Newmark finite difference method. The FG cylinder is assumed to be under axisymmetric and plane strain conditions. The mechanical properties of FGM are nonlinearly graded along the radial direction. A weak formulation for the set of coupled governing equations is transformed into local integral equations on local subdomains by using a Heaviside test function. All nodal points are regularly distributed along the thickness of the FG cylinder in radial direction and each node is located in a uni-directional subdomain to which a local integral equation is applied. The distributions of the temperature and radial displacements as well as the time history of them are obtained for some grading patterns of FGM at several time instants and for some COVs. The propagation of thermal and elastic waves along the radial direction in the FG thick hollow cylinder as well as the statistical characteristics of the variance and maximum values of the temperature and displacement are discussed in details.

[1] Industrial Engineering Department, Engineering Faculty, Ferdowsi University of Mashhad, Mashhad, Iran.
[2] Civil Engineering Department, Engineering Faculty, Ferdowsi University of Mashhad, Mashhad, Iran.
[3] Institute of Construction and Architecture, Slovak Academy of Sciences, 84503 Bratislava, Slovakia.

Keywords: Functionally graded materials, stochastic MLPG, thermo-elastic wave propagation, coupled thermo-elasticity.

1 Introduction

Safe and reliable design for FG structures under thermo-mechanical shock loadings or structures subjected to transient boundary conditions requires the engineering parameters to be considered as uncertain and random variables obeying physical conditions during manufacturing processes of materials. Some of the most important parameters, which are considered as input parameters in some engineering problems, are mechanical properties such as modulus of elasticity, density and heat transfer coefficients. The uncertain mechanical properties can be randomly generated using the Monte Carlo simulation with various coefficients of variations (COVs) and normal distribution. The stochastic analysis of dynamic problems as well as wave propagation in FG structures is helpful for prediction of all possible responses caused by uncertainties of mechanical properties. In recent years, several research works have been carried out in various topics dealing with uncertainty of engineering parameters such as mechanical properties that some of them are addressed in the following paragraphs.

The stochastic analysis of elastic buckling considering independent random Young's modulus and Poisson's ratio was carried out in a FG plates by Yang, Liew and Kitipornchai (2005a). In another work, the flexural deflection was stochastically studied in FG plates with various boundary conditions by Yang, Liew and Kitipornchai (2005b). In those works, the FG plate was subjected to static loading. The response of the FG plate under thermal boundary conditions was analyzed considering uncertain and random parameters for component volume fractions and the porosity using non-Gaussian simulation technique by Ferrante and Graham-Brady (2005). Kitipornchai, Yang and Liew (2005) obtained the vibration frequencies for FG laminates subjected to various and general boundary conditions using the mean-centered first-order perturbation technique for random free vibration. Rahman and Chakraborty (2007) presented a new stochastic finite element method to predict the probabilistic characteristics of elastic mechanical model in functionally graded materials (FGMs). The stochastic finite element method was applied also to solution of partial differential equations in one dimensional and time dependent conditions with uncertain coefficients by Saleh, El-Kalla and Ehab (2007). A stochastic analytical method with Monte Carlo simulation was presented to analyze the thermo-elastic response in functionally graded plate under random temperature loads [Chiba and Sugano (2007)] and with uncertain material properties [Chiba and Sugano (2008)] as well as for functionally graded annular disc with variable and/or constant thickness and random heat transfer coefficients by Chiba (2009). Shaker

et al. (2008) employed the stochastic finite element method for free vibration and fundamental frequency sensitivity stochastic analyses assuming uncertainty in material parameters. Chakraborty and Rahman (2008) presented an analytical method based on three stochastic multi-scale models including sequential, invasive, and concurrent models for the crack stochastic analysis in functionally graded composites. The applicability of the presented analytical method was compared with the results obtained using the direct Monte Carlo simulation. To have safe and reliable design in FG thick hollow cylinder subjected to shock loading, hybrid numerical methods with Monte Carlo simulation were developed for the dynamic responses [Shahabian and Hosseini (2010)] and stress field reliability [Hosseini and Shahabian (2010)] with assuming Gaussian distribution for uncertain constitutive mechanical properties of FGMs.

In the last decade, the Meshless local Petrov-Galerkin method (MLPG) proved to be one of the most efficient numerical methods in engineering problems. In this method, the analyzed domain is considered to be covered by small subdomains which are randomly distributed and local (symmetric or unsymmetric) weak forms integrations are considered over these subdomains. Based on the MLPG method, some works on thermo-elasticity and heat conduction problems in isotropic and functionally graded materials were carried out by researchers in the recent years. The meshless local Petrov-Galerkin (MLPG) method was deeply investigated for many meshless formulations with trial and test functions from various functional spaces by [Atluri (2004)]. The application of local integral equations and also MLPG method can be found to solve the governing equations on elastodynamic analysis [Sladek et al. (2003a and 2003b)], heat conduction and temperature field analysis [Sladek et al. (2003c, 2003d and 2005)], uncoupled thermo-elasticity [Sladek et al. (2001)] and coupled thermo-elasticity [Sladek et al. (2006) and Hosseini et al. (2011)] in homogeneous and nonhomogeneous solids. The MLPG method was successfully employed also for 3D transient heat conduction problems in materials with continuously non-homogeneous and anisotropic properties [Sladek et al (2008a)]. One of the most important topics in designing and engineering purposes for functionally graded materials (FGMs) is wave propagation analysis in the FG structures under shock loading in both displacement (elastic wave) and temperature (thermal wave) fields. The study of wave propagation phenomena is based on the coupled thermo-elasticity for which several theories have been developed. The Green-Naghdi (GN) theory seems to be the best realistic one of them. In GN theory, the wave propagation speed can be estimated in both temperature and displacement fields.

In this article, the effects of uncertainty in constitutive mechanical properties for functionally graded thick hollow cylinder are studied. The mechanical properties of

FGM are considered to be random variables, which are generated using the Monte Carlo simulation with proper coefficients of variations (COVs). To find the thermo-elastic waves and dynamic behaviors of temperature and displacement fields, the stochastic coupled governing equations based on Green-Naghdi theory of thermo-elasticity are solved using the meshless local Petrov-Galerkin (stochastic MLPG) method accompanied by the Newmark finite difference method for discretizing the time. In the presented work, the FG cylinder is supposed to be axisymmetric and with translational symmetry along its infinite length (plane strain conditions). After substitution of spatial approximations into the local integral equations of coupled thermo-elasticity governing equations, a system of ordinary differential equations (ODE) is obtained. The system of the ODE is solved by the Newmark finite difference method. The time history of maximum and variance of temperature and displacement fields are obtained for several grading patterns and coefficients of variations (COVs). The effects of uncertainty on thermo-elastic wave propagation along the radial direction are studied for various grading patterns of FGM in which the mechanical properties vary as nonlinear function of radius in volume fraction form. The frequency histogram, cumulative frequency histogram and cumulative distribution function of temperature and radial displacement are calculated for some volume fraction exponents, COVs and time intervals.

2 Stochastic coupled thermo-elasticity equations

A model in coupled thermo-elasticity, which is called the GN theory of thermo-elasticity, was presented by Green and Naghdi (1993). The governing equations of motion and heat conduction based on the GN theory of linear thermo-elasticity without energy dissipation for isotropic and non-homogeneous medium are given as

$$\nabla \cdot \sigma + \rho \mathbf{F} = \rho \ddot{\mathbf{u}} \tag{1}$$

$$c\,\ddot{T} + \gamma T_0 \nabla \cdot \ddot{\mathbf{u}} = \rho\,\dot{g} + \nabla \cdot (k^* \nabla T) \tag{2}$$

where σ is the stress tensor whose Cartesian components are given as

$$\sigma_{ij} = \delta_{ij}(\lambda u_{k,k} - \gamma T) + \mu(u_{i,j} + u_{j,i})$$

$\mathbf{u}$ is the displacement vector, T is the temperature fluctuation around the uniform reference temperature T_0, $\mathbf{F}$ is the density of external forces and $\dot{g}$ is the rate of external supply of heat. Both the $\mathbf{F}$ and $\dot{g}$ are assumed to be absent in this work. Furthermore, ρ is the mass density, c is the specific heat, λ and μ are the Lame constants and

$$\gamma = (3\lambda + 2\mu)\,\beta^* \tag{3}$$

whereβ^* is the coefficient of linear thermal expansion and $k^*$is a material parameter of the GN theory. The coupled equations (1) and (2) can be rewritten into the stochastic form as follows

$$\nabla \cdot \sigma + \tilde{\rho}\mathbf{F} = \tilde{\rho}\ddot{\mathbf{u}} \tag{4}$$

$$\tilde{c}\ddot{T} + \tilde{\gamma}T_0 \nabla \cdot \ddot{\mathbf{u}} = \tilde{\rho}\,\dot{g} + \nabla \cdot \left(\tilde{k}^* \nabla T\right) \tag{5}$$

with

$$\sigma_{ij} = \delta_{ij}(\tilde{\lambda}u_{k,k} - \tilde{\gamma}T) + \tilde{\mu}(u_{i,j} + u_{j,i})$$

$$\tilde{\gamma} = \left(3\tilde{\lambda} + 2\tilde{\mu}\right)\tilde{\beta}^*$$

where the tilde stands for stochastic parameters that are generated as random variables.

In what follows, we shall be interested in the thermoelastic problems in a cylindrical domain. Therefore the cylindrical coordinates and components appear to be appropriate. Assuming the axial symmetry as well as the translational symmetry along the infinitely long cylinder, we conclude that all physical quantities are independent on the angular and axial coordinates and

$$u_\theta = 0, \quad u_z = 0, \quad \sigma_{rr} = 2\tilde{\mu}u_{r,r} + \left(\tilde{\lambda}e - \tilde{\gamma}T\right), \quad \sigma_{\theta\theta} = 2\tilde{\mu}u_r/r + \left(\tilde{\lambda}e - \tilde{\gamma}T\right),$$

$$\sigma_{zz} = \tilde{\lambda}e - \tilde{\gamma}T, \quad \sigma_{r\theta} = 0 = \sigma_{rz} = \sigma_{z\theta}, \quad e = u_{r,r} + u_r/r$$

The governing equations (4) and (5) are reduced to the equations

$$\sigma_{rr,r} + \frac{1}{r}(\sigma_{rr} - \sigma_{\theta\theta}) - \tilde{\rho}\ddot{u}_r = -\tilde{\rho}F_r \tag{6}$$

$$\tilde{c}\ddot{T} + \tilde{\gamma}T_0\left(\ddot{u}_{r,r} + \frac{\ddot{u}_r}{r}\right) - \left(\tilde{k}^* T_{,r}\right)_{,r} - \frac{\tilde{k}^*}{r}T_{,r} = \tilde{\rho}\,\dot{g} \quad . \tag{7}$$

Assuming $F_r = 0$, $\dot{g} = 0$ and having used the following non-dimensional parameters

$$\bar{r} = \frac{r}{l}$$

$$\bar{t} = \frac{v}{l}t,\ \tilde{\kappa} = \frac{\tilde{k}^*}{\tilde{k}_0^*} \tag{8}$$

as well as non-dimensional field variables

$$\bar{\mathbf{u}} = \frac{\tilde{\lambda}_0 + 2\tilde{\mu}_0}{l\tilde{\gamma}_0 T_0}\mathbf{u}, \quad \bar{T} = \frac{T}{T_0},$$

$$\bar{\sigma}_{rr} = \frac{\sigma_{rr}}{\tilde{\gamma}_0 T_0}, \quad \bar{\sigma}_{\theta\theta} = \frac{\sigma_{\theta\theta}}{\tilde{\gamma}_0 T_0} \tag{9}$$

the governing equations become

$$\frac{\partial \bar{\sigma}_{rr}}{\partial \bar{r}} + \frac{1}{\bar{r}}(\bar{\sigma}_{rr} - \bar{\sigma}_{\theta\theta}) - \frac{1}{\tilde{c}_p^2}\frac{\partial^2 \bar{u}_r}{\partial \bar{t}^2} = 0 \tag{10}$$

$$\left(\frac{\partial}{\partial \bar{r}} + \frac{1}{\bar{r}}\right)\left(\tilde{\kappa}\frac{\partial \bar{T}}{\partial \bar{r}}\right) - \frac{1}{\tilde{c}_T^2}\frac{\partial^2 \bar{T}}{\partial \bar{t}^2} - \frac{1}{\tilde{c}_\varepsilon^2}\left(\frac{\partial}{\partial \bar{r}} + \frac{1}{\bar{r}}\right)\frac{\partial^2 \bar{u}_r}{\partial \bar{t}^2} = 0. \tag{11}$$

Note that "l" is a characteristic length and "v" is a characteristic speed, while

$$\tilde{\lambda}_0 = 2\tilde{\mu}_0 \frac{\nu}{1-2\nu}, \quad \tilde{\mu}_0 = \tilde{E}_0/2(1+\nu), \quad \tilde{\gamma}_0 = \left(3\tilde{\lambda}_0 + 2\tilde{\mu}_0\right)\tilde{\beta}_0^*,$$

$$\tilde{C}_p^2 = \frac{\tilde{\lambda}_0 + 2\tilde{\mu}_0}{\tilde{\rho}\, v^2}, \quad \tilde{C}_T^2 = \frac{\tilde{k}_0^*}{\tilde{c}\, v^2}, \quad \tilde{C}_\varepsilon^2 = \frac{\tilde{k}_0^*(\tilde{\lambda}_0 + 2\tilde{\mu}_0)}{\tilde{\gamma}\tilde{\gamma}_0 T_0\, v^2} \tag{12}$$

with ν being the Poisson ratio, E_0, β_0^* and k_0^* are certain values of the Young modulus, linear thermal expansion coefficient and k^*-parameter, respectively, say taken on the inner surface of the cylinder.

In coupled thermo-elasticity analysis, the Monte Carlo method is suggested to be used since the analytical solution is not available and the stochastic domain cannot be expressed or approximated by an analytical form. In the Monte Carlo estimation, the probability of uncertain parameters P_f which are greater than mean value can be calculated as

$$P_f = \frac{n}{N}$$

where N is the total number of simulations and n is the number of simulations which have greater values than the value for deterministic inputs (mean values of random variables).

The uncertain mechanical properties of FG cylinder, such as Young's modulus $\tilde{E}$, the mass density$\tilde{\rho}$, the thermal expansion coefficient $\tilde{\beta}^*$, the coefficient $\tilde{k}^*$ and the specific heat $\tilde{c}$ are graded along the thickness of cylinder. The radial distribution of material properties is shown by

$$\tilde{P} = \left(\tilde{P}_{out} - \tilde{P}_{in}\right)\left(\frac{\bar{r} - \bar{r}_{in}}{\bar{r}_{out} - \bar{r}_{in}}\right)^{\psi} + \tilde{P}_{in} \tag{13}$$

where $\tilde{P}$ is material property, ψ is a non-negative volume fraction exponent and subscripts "*in*" and "*out*" stand for quantities on the inner and outer surfaces of FG cylinder, respectively.

3 Meshless technique

As the first step in MLPG method, we have to determine the analyzed domain for the problem. All physical fields are dependent only on the radial coordinate due to the axial and translational symmetry in the presented problem. Consequently, in this problem, the analyzed domain is considered to be an abscissa along the radial coordinate of the FG cylinder. Some small subdomains with finite size in line segments form are distributed on the analyzed domain. Nodal points are randomly distributed in the global domain and each interior node $\bar{r}_I$ is surrounded by a subdomain (line segment) $\Omega_I = [\bar{r}_{I0}, \bar{r}_{I1}]$ on which a local weak formulation for the set of Green-Naghdi coupled thermoleasticity governing equations (10) and (11) is considered. Nevertheless, the balance equations should be satisfied over the actual physical subdomain which is the hollow cylinder of thickness $(\bar{r}_{I1} - \bar{r}_{I0})$ and finite height [Sladek et al 2008b]. Since the integrands are independent on the angular and axial coordinates, the integrations with respect to these coordinates are trivial and it remains to integrate along the radial coordinate over the subdomain Ω_I The local weak form of coupled equations over the subdomain Ω_I can be written using test functions $h(\bar{r})$ for displacement field and $g(\bar{r})$ for temperature field

$$\int_{\Omega_I} \left\{ \frac{\partial \bar{\sigma}_{rr}}{\partial \bar{r}} + \frac{1}{\bar{r}} (\bar{\sigma}_{rr} - \bar{\sigma}_{\theta\theta}) - \frac{1}{\tilde{c}_p^2} \frac{\partial^2 \bar{u}_r}{\partial \bar{t}^2} \right\} h(\bar{r})\, \bar{r}\, d\bar{r} = 0 \tag{14}$$

$$\int_{\Omega_I} \left\{ \left(\frac{\partial}{\partial \bar{r}} + \frac{1}{\bar{r}} \right) \left(\tilde{\kappa} \frac{\partial \bar{T}}{\partial \bar{r}} \right) - \frac{1}{\tilde{c}_T^2} \frac{\partial^2 \bar{T}}{\partial \bar{t}^2} - \frac{1}{\tilde{c}_\varepsilon^2} \left(\frac{\partial}{\partial \bar{r}} + \frac{1}{\bar{r}} \right) \frac{\partial^2 \bar{u}_r}{\partial \bar{t}^2} \right\} g(\bar{r})\, \bar{r}\, d\bar{r} = 0 \tag{15}$$

for all interior nodes $I = 1, 2, ..., n$. Using the integration by parts technique, the equations (14) and (15) can be rewritten in the following forms

$$\bar{r} \bar{\sigma}_{rr} h(\bar{r}) \Big|_{\bar{r}_{I0}}^{\bar{r}_{I1}} - \int_{\bar{r}_{I0}}^{\bar{r}_{I1}} \left\{ \left(\bar{\sigma}_{\theta\theta} + \frac{\bar{r}}{\tilde{c}_p^2} \frac{\partial^2 \bar{u}_r}{\partial \bar{t}^2} \right) h(\bar{r}) + \bar{r} \bar{\sigma}_{rr} \frac{\partial h(\bar{r})}{\partial \bar{r}} \right\} d\bar{r} = 0$$

$$\bar{r} \left[\tilde{\kappa} \frac{\partial \bar{T}}{\partial \bar{r}} - \frac{1}{\tilde{c}_\varepsilon^2} \frac{\partial^2 \bar{u}_r}{\partial \bar{t}^2} \right] g(\bar{r}) \Big|_{\bar{r}_{I0}}^{\bar{r}_{I1}} - \int_{\bar{r}_{I0}}^{\bar{r}_{I1}} \left\{ \bar{r} \left[\tilde{\kappa} \frac{\partial \bar{T}}{\partial \bar{r}} \frac{\partial g(\bar{r})}{\partial \bar{r}} - \frac{\partial^2 \bar{u}_r}{\partial \bar{t}^2} \frac{\partial}{\partial \bar{r}} \left(\frac{g(\bar{r})}{\tilde{c}_\varepsilon^2} \right) \right] + \right.$$

$$\left. + \frac{\bar{r} g(\bar{r})}{\tilde{c}_T^2} \frac{\partial^2 \bar{T}}{\partial \bar{t}^2} \right\} d\bar{r} = 0 \tag{16}$$

We shall consider the Heaviside unit step function for the test functions $h(\bar{r})$ and

$g(\bar{r})$ in each subdomain

$$h(\bar{r}) = g(\bar{r}) = \begin{cases} 1 & at \quad \bar{r} \in \Omega_I \\ 0 & at \quad \bar{r} \notin \Omega_I \end{cases}$$

The local integral equations (16) and (17) are simplified as

$$\bar{r}\bar{\sigma}_{rr}|_{\bar{r}_{I0}}^{\bar{r}_{I1}} - \int_{\bar{r}_{I0}}^{\bar{r}_{I1}} \left(\bar{\sigma}_{\theta\theta} + \frac{\bar{r}}{\tilde{c}_p^2} \frac{\partial^2 \bar{u}_r}{\partial \bar{t}^2} \right) d\bar{r} = 0 \tag{17}$$

$$\bar{r}\left[\tilde{\kappa} \frac{\partial \bar{T}}{\partial \bar{r}} - \frac{1}{\tilde{c}_\varepsilon^2} \frac{\partial^2 \bar{u}_r}{\partial \bar{t}^2} \right] \Bigg|_{\bar{r}_{I0}}^{\bar{r}_{I1}} - \int_{\bar{r}_{I0}}^{\bar{r}_{I1}} \bar{r}\left[\frac{1}{\tilde{c}_T^2} \frac{\partial^2 \bar{T}}{\partial \bar{t}^2} - \frac{\partial^2 \bar{u}_r}{\partial \bar{t}^2} \frac{\partial}{\partial \bar{r}} \left(\frac{1}{\tilde{c}_\varepsilon^2} \right) \right] d\bar{r} = 0 \tag{18}$$

Using the radial basis functions (RBFs), the field variables $\bar{u}(\bar{r},\bar{t})$ and $\bar{T}(\bar{r},\bar{t})$ are spatially distributed over a number of randomly located nodes $\bar{r}_I$, $I = 1,2,...,n$ employing the meshless approximation. Consequently, we will use the following approximations for the temperature and displacement fields

$$\bar{u}(\bar{r},\bar{t}) = R^T(\bar{r})\,\alpha(\bar{t}) \tag{19}$$

$$\bar{T}(\bar{r},\bar{t}) = R^T(\bar{r})\,\beta(\bar{t}) \tag{20}$$

where $R^T(\bar{r}) = [R_1(\bar{r}), R_2(\bar{r}), ..., R_n(\bar{r})]$ is the set of radial basis functions centered around $\bar{r}_I$, and α and β are vectors containing the time-dependent coefficients of α_I and β_I, $I = 1,2,...,n$. In this article, we use the multiquadric form of radial basis functions, which can be defined as

$$R_I(\bar{r}) = \left(|\bar{r} - \bar{r}_I|^2 + c^2 \right)^{m/2} \tag{21}$$

To find the terms α and β, the aforementioned interpolation equations (20) and (21) should be solved using following system of linear equations.

$$R_0\,\alpha(\bar{t}) = \hat{u}(\bar{t}) \tag{22}$$

$$R_0\,\beta(\bar{t}) = \hat{T}(\bar{t}) \tag{23}$$

where

$$\hat{T}^T(\bar{t}) = \left[\bar{T}^1(\bar{t}), \bar{T}^2(\bar{t}), ..., \bar{T}^n(\bar{t}) \right] \tag{24}$$

$$\hat{u}^T(\bar{t}) = \left[\bar{u}^1(\bar{t}), \bar{u}^2(\bar{t}), ..., \bar{u}^n(\bar{t}) \right] \tag{25}$$

are composed of the time variable nodal values of displacements $\bar{u}^I(\bar{t})$ and temperature $\bar{T}^I(\bar{t})$, while R_0 is the matrix defined by nodal values of the RBFs as

$$R_0 = \begin{bmatrix} R_1(\bar{r}_1) & R_2(\bar{r}_1) & \ldots & R_n(\bar{r}_1) \\ R_1(\bar{r}_2) & R_2(\bar{r}_2) & \ldots & R_n(\bar{r}_2) \\ \vdots & \vdots & \vdots & \vdots \\ R_1(\bar{r}_n) & R_2(\bar{r}_n) & \ldots & R_n(\bar{r}_n) \end{bmatrix} \tag{26}$$

The vectors $\alpha(\bar{t})$ and $\beta(\bar{t})$can be calculated using following equations

$$\alpha(\bar{t}) = R_0^{-1}\hat{u}(\bar{t}) \tag{27}$$

$$\beta(\bar{t}) = R_0^{-1}\hat{T}(\bar{t}) \tag{28}$$

The approximated functions can be expressed in terms of the nodal values and the shape functions as

$$\bar{u}(\bar{r},\bar{t}) = R^T(\bar{r})R_0^{-1}\hat{u}(\bar{t}) = \Phi^T(\bar{r})\hat{u}(\bar{t}) = \sum_{a=1}^{n}\phi^a(\bar{r})\bar{u}^a(\bar{t}) \tag{29}$$

$$\bar{T}(\bar{r},\bar{t}) = R^T(\bar{r})R_0^{-1}\hat{T}(\bar{t}) = \Phi^T(\bar{r})\hat{T}(\bar{t}) = \sum_{a=1}^{n}\phi^a(\bar{r})\bar{T}^a(\bar{t}) \tag{30}$$

where $\phi^a(\bar{r})$ is the shape function associated with the node a. The nodal shape functions are given by

$$\Phi^T(\bar{r}) = R^T(\bar{r})R_0^{-1} \tag{31}$$

Assuming the Poisson ratio to be constant and bearing in mind the definitions of dimensionless stresses, in view of the approximations (30) and (31), we obtain the approximations for stress tensor components

$$\bar{\sigma}_{rr}(\bar{r}) = \frac{\tilde{E}(\bar{r})}{\tilde{E}_0}\sum_{a=1}^{n}\left[\left(\frac{\partial\phi^a(\bar{r})}{\partial\bar{r}} + \frac{\nu}{1-\nu}\frac{\phi^a(\bar{r})}{\bar{r}}\right)\bar{u}^a(\bar{t}) - \frac{\tilde{\beta}^*(\bar{r})}{\tilde{\beta}_0^*}\bar{T}^a(\bar{t})\right] \tag{32}$$

$$\bar{\sigma}_{\theta\theta}(\bar{r}) = \frac{\tilde{E}(\bar{r})}{\tilde{E}_0}\sum_{a=1}^{n}\left[\left(\frac{\nu}{1-\nu}\frac{\partial\phi^a(\bar{r})}{\partial\bar{r}} + \frac{\phi^a(\bar{r})}{\bar{r}}\right)\bar{u}^a(\bar{t}) - \frac{\tilde{\beta}^*(\bar{r})}{\tilde{\beta}_0^*}\bar{T}^a(\bar{t})\right] \quad . \tag{33}$$

Now, we can collocate the prescribed boundary conditions on the surface of the cylinder and at the interior nodes, we shall consider the discretized local integral equations (18) and (19) given as

$$\sum_{a=1}^{n} \bar{u}^a(\bar{t}) \left\{ \tilde{E}(\bar{r}) \left(\bar{r} \frac{\partial \phi^a(\bar{r})}{\partial \bar{r}} + \frac{\nu}{1-\nu} \phi^a(\bar{r}) \right) \Big|_{\bar{r}_{I0}}^{\bar{r}_{I1}} - \int_{\bar{r}_{I0}}^{\bar{r}_{I1}} \tilde{E}(\bar{r}) \left(\frac{\nu}{1-\nu} \frac{\partial \phi^a(\bar{r})}{\partial \bar{r}} + \frac{\phi^a(\bar{r})}{\bar{r}} \right) d\bar{r} \right\} -$$

$$- \sum_{a=1}^{n} \ddot{\bar{u}}^a(\bar{t}) \int_{\bar{r}_{I0}}^{\bar{r}_{I1}} \frac{\bar{r} \tilde{E}_0}{\tilde{c}_p^2(\bar{r})} \phi^a(\bar{r}) d\bar{r} -$$

$$- \sum_{a=1}^{n} \bar{T}^a(\bar{t}) \left\{ \bar{r} \tilde{E}(\bar{r}) \frac{\tilde{\beta}^*(\bar{r})}{\tilde{\beta}_0^*} \phi^a(\bar{r}) \Big|_{\bar{r}_{I0}}^{\bar{r}_{I1}} - \int_{\bar{r}_{I0}}^{\bar{r}_{I1}} \tilde{E}(\bar{r}) \frac{\tilde{\beta}^*(\bar{r})}{\tilde{\beta}_0^*} \phi^a(\bar{r}) d\bar{r} \right\} = 0 \tag{34}$$

$$\sum_{a=1}^{n} \ddot{\bar{u}}^a(\bar{t}) \left\{ - \frac{\bar{r}}{\tilde{c}_\varepsilon^2(\bar{r})} \phi^a(\bar{r}) \Big|_{\bar{r}_{I0}}^{\bar{r}_{I1}} + \int_{\bar{r}_{I0}}^{\bar{r}_{I1}} \bar{r} \phi^a(\bar{r}) \frac{\partial \tilde{c}_\varepsilon^{-2}}{\partial \bar{r}} d\bar{r} \right\} - \sum_{a=1}^{n} \ddot{\bar{T}}^a(\bar{t}) \int_{\bar{r}_{I0}}^{\bar{r}_{I1}} \frac{\bar{r}}{\tilde{c}_T^2(\bar{r})} \phi^a(\bar{r}) d\bar{r} +$$

$$+ \sum_{a=1}^{n} \bar{T}^a(\bar{t}) \, \tilde{\kappa}(\bar{r}) \bar{r} \frac{\partial \phi^a(\bar{r})}{\partial \bar{r}} \Big|_{\bar{r}_{I0}}^{\bar{r}_{I1}} = 0 \quad . \tag{35}$$

It should be noted that the essential boundary conditions on $\partial \Omega_s$can be imposed directly using the interpolation approximation (30) and (31). In this regards, we consider the following thermal shock applied on inner surface of FG cylinder as boundary condition. The inner surface of cylinder is assumed to be under thermal shock and simply supported conditions for displacements, which can be defined as follows. At inner surface we have

$$\bar{T}\left(\bar{r}_{in}, \bar{t}\right) = H\left(\bar{t}\right), \quad \bar{u}\left(\bar{r}_{in}, \bar{t}\right) = 0 \tag{36}$$

and for outer surface, we can write

$$\bar{T}\left(\bar{r}_{out}, \bar{t}\right) = 0, \quad \bar{u}\left(\bar{r}_{out}, \bar{t}\right) = 0 \tag{37}$$

where $H(\bar{t})$ is the Heaviside unit step function. We use the interpolation approximation on boundary conditions as follows

$$\bar{T}\left(\bar{r}_{in}, \bar{t}\right) = \sum_{a=1}^{n} \phi^a\left(\bar{r}_{in}\right) \bar{T}^a\left(\bar{t}\right) = H\left(\bar{t}\right) \tag{38}$$

$$\bar{u}\left(\bar{r}_{in},\bar{t}\right)=\sum_{a=1}^{n}\phi^{a}\left(\bar{r}_{in}\right)\bar{u}^{a}\left(\bar{t}\right)=0 \tag{39}$$

$$\bar{T}\left(\bar{r}_{out},\bar{t}\right)=\sum_{a=1}^{n}\phi^{a}\left(\bar{r}_{out}\right)\bar{T}^{a}\left(\bar{t}\right)=0 \tag{40}$$

$$\bar{u}\left(\bar{r}_{out},\bar{t}\right)=\sum_{a=1}^{n}\phi^{a}\left(\bar{r}_{out}\right)\bar{u}^{a}\left(\bar{t}\right)=0 \tag{41}$$

The homogeneous initial conditions will be assumed in this paper, i.e.

$$\bar{u}_r(\bar{r},\bar{t}=0)=0,\quad \dot{\bar{u}}_r(\bar{r},\bar{t}=0)=0,\quad \bar{T}(\bar{r},\bar{t}=0)=0,\quad \dot{\bar{T}}(\bar{r},\bar{t}=0)=0.$$

In view of the considered spatial interpolations, the discretized boundary conditions and the integral equations on local sub-domains can be written in the matrix form as a system of ordinary differential equations (ODEs) for the time dependent nodal values of the displacement and temperature.

$$[M]\left\{\ddot{\eta}\right\}+[K]\left\{\eta\right\}=[f] \tag{42}$$

where

$$\left\{\eta\right\}=\left\{\begin{array}{c}\left[\hat{u}\left(\bar{t}\right)\right]\\ \left[\hat{T}\left(\bar{t}\right)\right]\end{array}\right\} \tag{43}$$

$$\hat{u}^{T}\left(\bar{t}\right)=\left[\bar{u}^{1}\left(\bar{t}\right),\bar{u}^{2}\left(\bar{t}\right),....,\bar{u}^{n}\left(\bar{t}\right)\right] \tag{44}$$

$$\hat{T}^{T}\left(\bar{t}\right)=\left[\bar{T}^{1}\left(\bar{t}\right),\bar{T}^{2}\left(\bar{t}\right),....,\bar{T}^{n}\left(\bar{t}\right)\right] \tag{45}$$

There are some numerical methods to solve the set of equations (43) in time domain. We use the well-known Newmark finite difference method with suitable time step in which the terms β and γ are selected equal to $\beta=0.25$ and $\gamma=0.5$ for the best convergence rate.

4 Numerical example and discussions

A functionally graded thick hollow cylinder is considered in axisymmetric and plane strain conditions with inner and outer radii $\bar{r}_{in}$ and $\bar{r}_{out}$, respectively. The thickness of cylinder can be calculated as $h=\bar{r}_{out}-\bar{r}_{in}$. All results for both the temperature and displacement fields are obtained for three values of coefficients of variations (COVs) as $COV=2.5\%$, $COV=5\%$ and $COV=10\%$. At first, in

order to verify the presented method and data, the volume fraction exponent is considered to be equal to zero$\psi = 0$. Consequently, the cylinder is considered as an isotropic and homogeneous thick cylinder and material properties throughout the cylinder are equal to the material properties on the outer surfaceP_{out}. The material properties are the same as in the published work by Taheri et al. (2005)

$$C_p = 0.5, \;\; C_T = 1.0, \;\; C_s = \sqrt{\frac{\mu}{\rho\, v^2}} = 0.267, \;\; \varepsilon^* = 0.073 \tag{46}$$

The prescribed initial and boundary conditions are specified in the previous section. The distribution of non-dimensional temperature across the thickness of the homogeneous cylinder (the same as in the published work by Taheri (2005)) can be seen for various COVs and deterministic inputs in Fig.1. The results for the cylinder with $COV = 0\%$, which means the deterministic data, should coincide with those of the previous work based on deterministic analysis [Taheri et al. (2005)]. It can be clearly seen in Fig.1 a good agreement in comparison between the results corresponding to deterministic inputs $COV = 0\%$ and published data. Moreover, Fig. 1 shows the influence of material coefficients variations (COVs) on temperature distribution along the thickness of cylinder.

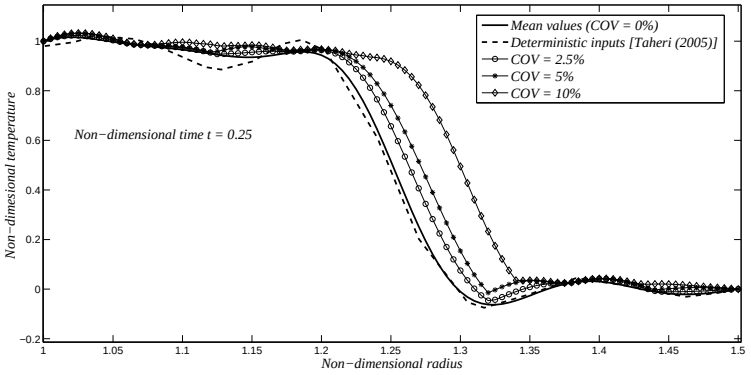

Figure 1: Comparison of non-dimensional temperature distribution for various COVs and published data [Taheri (2005)] in homogeneous cylinder.

In order to investigate the influence of uncertainty in FGMs on thermo-elastic wave propagation, the following non-dimensional material parameters are considered as mean values of random variables, which are generated using the Monte Carlo simulation with various (COVs):

$$(C_p)_{in}^{mean} = 0.7, \;\; (C_T)_{in}^{mean} = 1.2, \;\; (C_s)_{in}^{mean} = 0.26, \;\; (\varepsilon^*)_{in}^{mean} = 0.07 \tag{47}$$

$$(C_p)_{out}^{mean} = 0.5, \quad (C_T)_{out}^{mean} = 1, \quad (C_s)_{out}^{mean} = 0.28, \quad (\varepsilon^*)_{out}^{mean} = 0.08 \tag{48}$$

In stochastic analysis of coupled thermo-elasticity, we have a set of outputs for the non-dimensional temperature and displacement in each investigation point on the thickness of the cylinder at various the time instants for the specified (COVs) and particular grading patterns of FGM. As a sample, the non-dimensional temperature in middle point of the thickness for $COV = 2.5\%$, $\psi = 0.5$ at the non-dimensional time $\bar{t} = 0.5$ is illustrated in Fig.2 using for example 100 samples. We can see the mean, maximum and minimum values for variation. In engineering design, the maximum values and also the values over the mean value should be considered in the design procedure. We find the thermo-elastic wave propagation and also the time history of both the displacement and temperature fields corresponding to maximum values of ... (WHAT ???). Additionally, some stochastic parameters are found for the problem based on the results of coupled thermo-elasticity analysis in FGM such as frequency histogram, cumulative frequency histogram and cumulative distribution functions (CDFs).

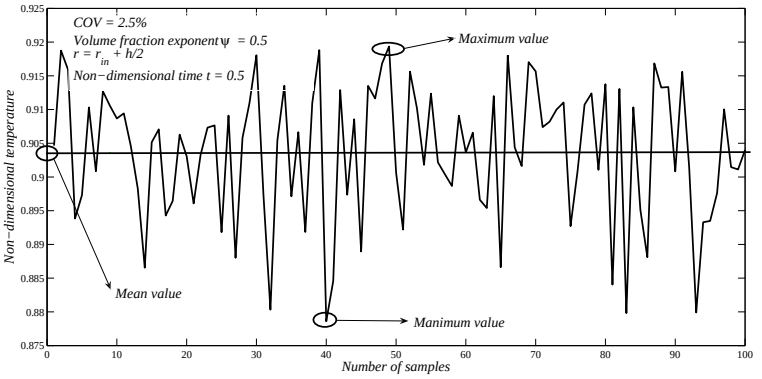

Figure 2: Variation of non-dimensional temperature versus number of simulations at middle point of thickness for certain "ψ", "$\bar{t}$" and "COV".

The frequency histogram of non-dimensional temperature at $r = r_{in} + 3h/4$ is shown in Fig.3 for a sample case specified by $\psi = 0.5$, $\bar{t} = 1.8$ and $COV = 5\%$. The distribution of sample values can be found using the frequency histogram, which can help us to obtain the cumulative frequency histogram and CDF.

The Fig.4 shows us a sample of the cumulative frequency histogram of non-dimensional temperature in $r = r_{in} + 3h/4$ for $\psi = 0.5$, $\bar{t} = 1.8$ and $COV = 5\%$. Using the histogram of cumulative frequency, the cumulative distribution function (CDF) can be

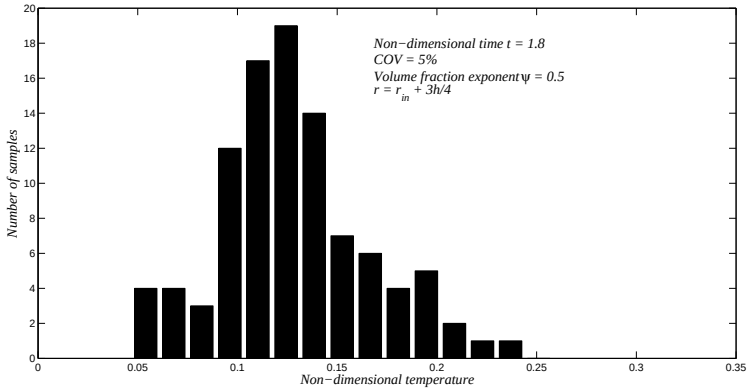

Figure 3: Frequency histogram of non-dimensional temperature for "$r = r_{in} + 3h/4$", "$\psi = 0.5$", "$\bar{t} = 1.8$" and "$COV = 5\%$".

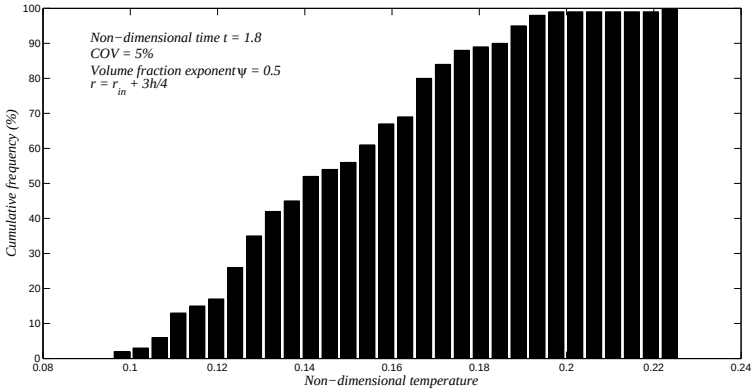

Figure 4: Cumulative frequency histogram of non-dimensional temperature for "$r = r_{in} + 3h/4$", "$\psi = 0.5$", "$\bar{t} = 1.8$" and "$COV = 5\%$".

obtained for various parameters such as volume fraction exponent ψ and COV in various points on thickness and at different time instants. The influence of COV on behavior of CDF can be found in Fig.5 for $r = r_{in} + h/2$, $\psi = 0.5$ and $\bar{t} = 0.5$.

It is concluded from Fig.5that with increasing the "COV"the CDF is becoming horizontally more stretched, which means the distribution of data is becoming wider. Using the presented method, we can find the CDF for other variation of parameters.

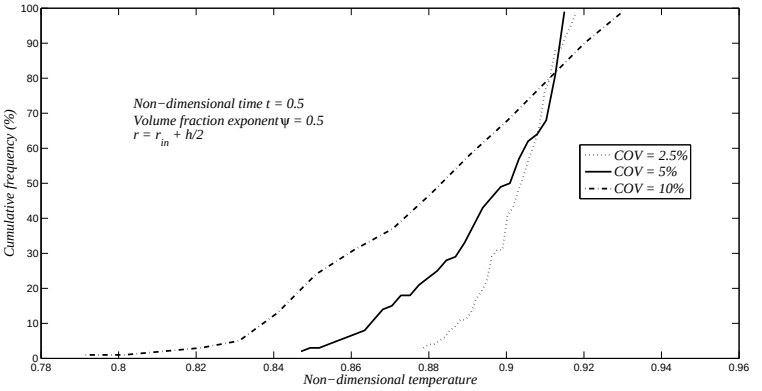

Figure 5: Cumulative distribution function (CDF) of non-dimensional temperature for various COV and $r = r_{in} + h/2$", "$\psi = 0.5$" and "$\bar{t} = 0.5$"

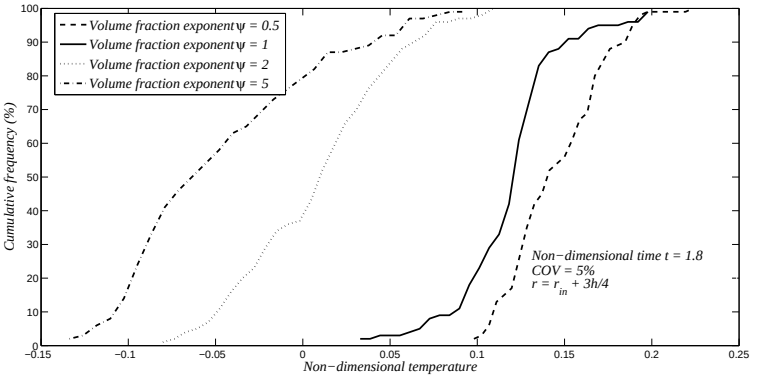

Figure 6: Cumulative distribution function (CDF) of non-dimensional temperature for various grading patterns in FGM and "$r = r_{in} + 3h/4$", "$\psi = 0.5$", "$\bar{t} = 1.8$" and "$COV = 5\%$".

The influence of various parameters on CDF can be helpful for designing procedure and probabilistic analysis of structures made of functionally graded materials.

By increasing the value of the volume fraction exponent, the CDF is stretching in the temperature domain. This phenomenon can be seen in Fig.6, which shows the cumulative distribution function for several values of the volume fraction exponent and $r = r_{in} + 3h/4$, $COV = 5\%$ and $\bar{t} = 1.8$. The width of the distribution of

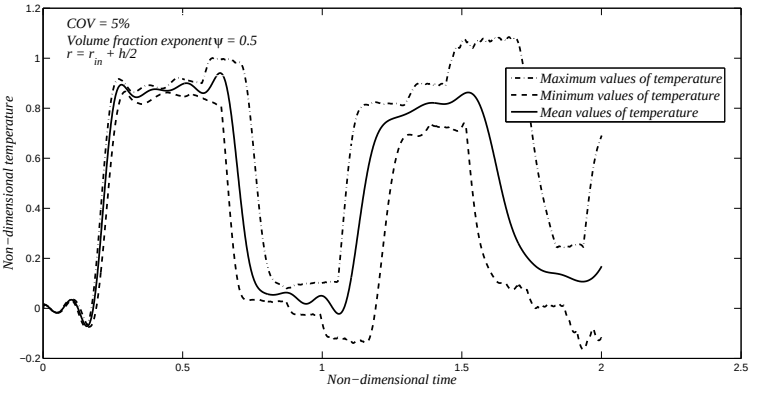

Figure 7: The time history of maximum, mean and minimum values of non-dimensional temperature for $r = r_{in} + h/2$", "$COV = 5\%$" and "$\bar{t} = 0.5$"

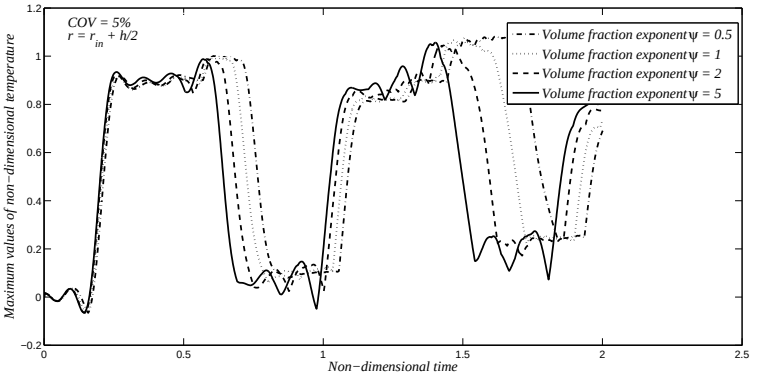

Figure 8: The time history of maximum values of non-dimensional temperature for various values of volume fraction exponent, $r = r_{in} + h/2$" and "$COV = 5\%$"

stochastic data for the temperature field is increasing with increasing the value of the volume fraction exponent ψ.

The time history of maximum, mean and minimum values of the non-dimensional temperature in the middle point of thickness is drawn in Fig.7 with taking $COV = 5\%$ and $\psi = 0.5$. If we consider the material properties as uncertain and random variables, the dynamic response of FG structures is highly affected by some statistical parameters such as COV. In other words, there is a significant difference

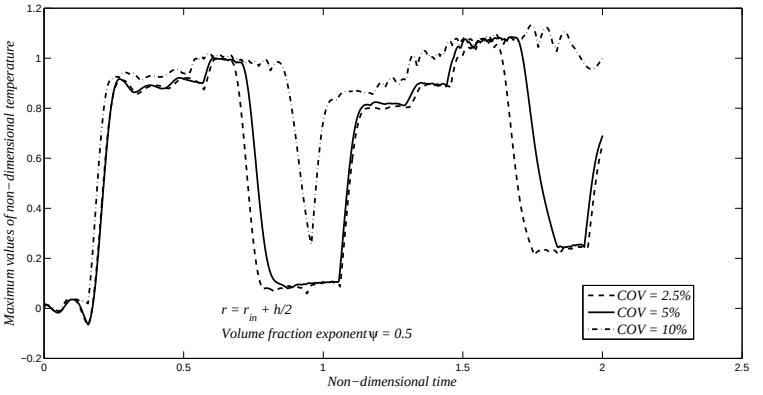

Figure 9: The time history of maximum values of non-dimensional temperature for various COV at middle point of thickness "$\psi = 0.5$".

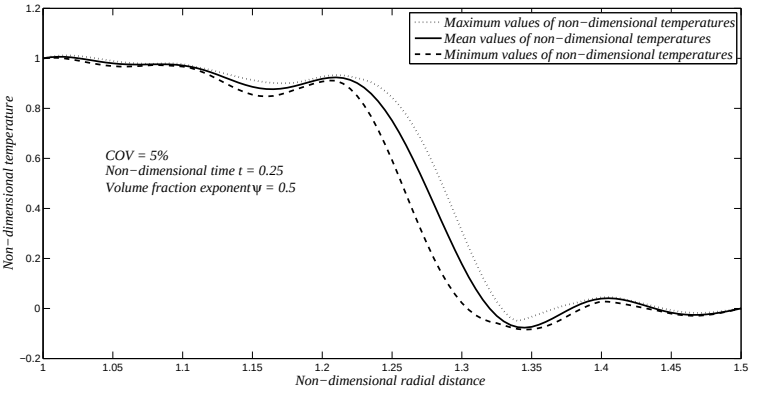

Figure 10: Non-dimensional temperature distribution across thickness of FG cylinder at "$\bar{t} = 0.25$" and "$\psi = 0.5$" and "$COV = 5\%$".

between the maximum and mean values at each time instant and any point on the thickness of the FG cylinder.

Consequently, the time history of maximum values of temperature should be considered for engineering calculations in designing purposes. The influence of the volume fraction exponent variation on the time history of maximum values of non-dimensional temperature can be observed in Fig.8. The period of time os-

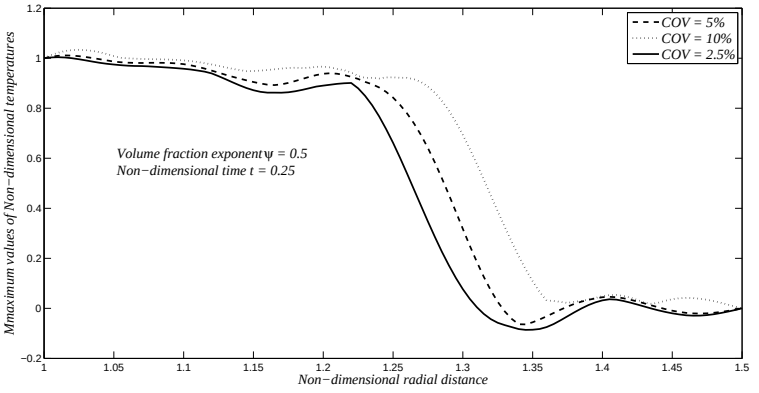

Figure 11: The distribution of maximum values of non-dimensional temperature across thickness of FG cylinder at "$\bar{t} = 0.25$" and "$\psi = 0.5$" and various COV.

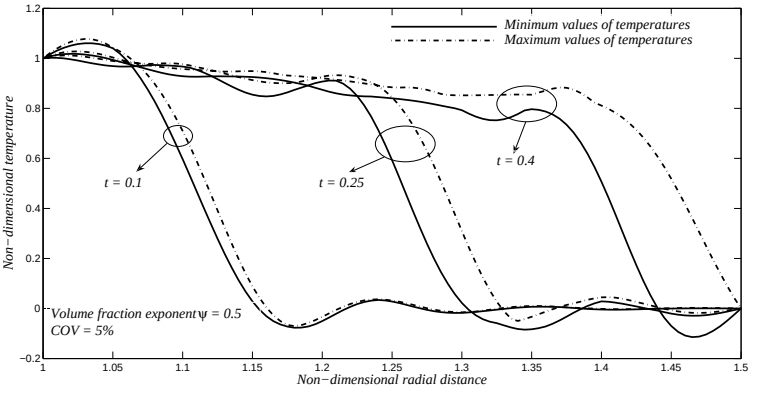

Figure 12: The propagation of thermal wave corresponding to maximum and minimum values along the radial direction for "$COV = 5\%$" and "$\psi = 0.5$".

cillations is increased with decreasing the value of ψ. The maximum values of non-dimensional temperature should increase with increasing the value of COV.

This phenomenon was verified by numerical results at each point along the thickness of the FG cylinder and it is illustrated for a sample with $\psi = 0.5$ at the middle point of the thickness in Fig.9. The distribution of the non-dimensional temperature along the thickness of the FG cylinder is plotted for several values of the COV

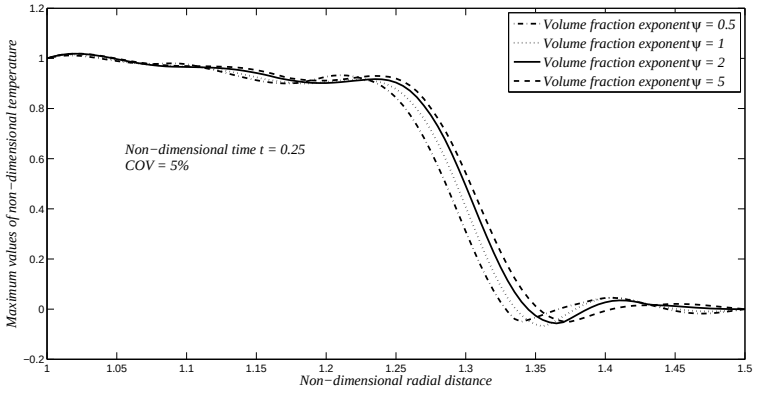

Figure 13: The distribution of non-dimensional temperature for various grading patterns of FGM and "$COV = 5\%$" and "$\bar{t} = 0.25$".

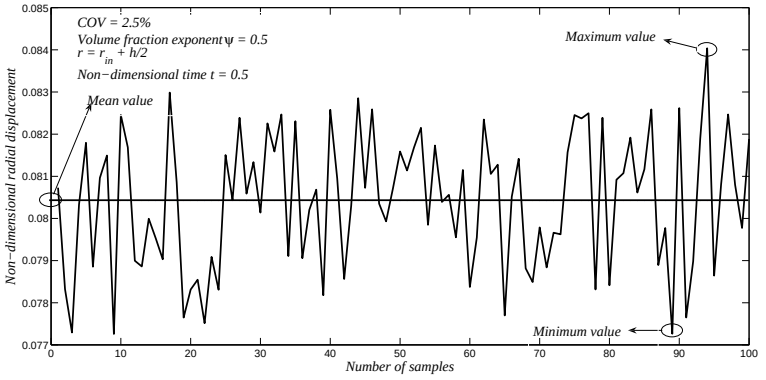

Figure 14: Variation of non-dimensional radial displacement versus number of simulations at middle point of thickness for certain "$\bar{t}$", "ψ" and "COV".

in Fig.10. It can be seen from Fig.10 that the position of the thermal wave front is different for maximum, mean and minimum values of the temperature field. Hence, we conclude again that the thermal wave corresponding to maximum values should be considered in design calculations.

The thermal wave fronts for bigger values of the COV should reach the outer bounding surface of the cylinder sooner than the wave fronts for smaller values of the COV, as can be seen on Fig.11 for $\bar{t} = 0.25$ and $\psi = 0.5$. The thermal wave propa-

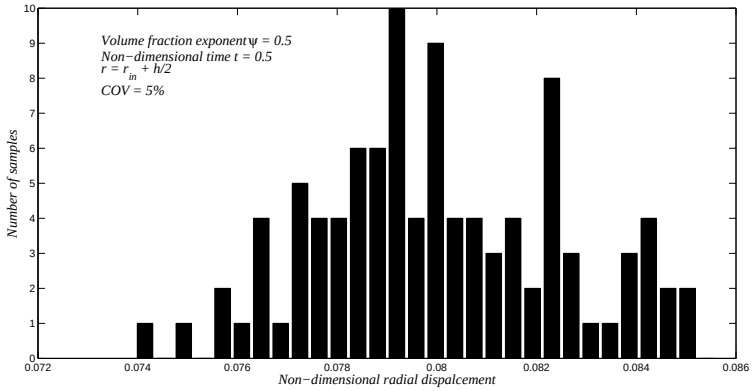

Figure 15: Frequency histogram of non-dimensional radial displacement at middle point of thickness for certain "$\psi = 0.5$", "$\bar{t} = 0.5$" and "$COV = 5\%$".

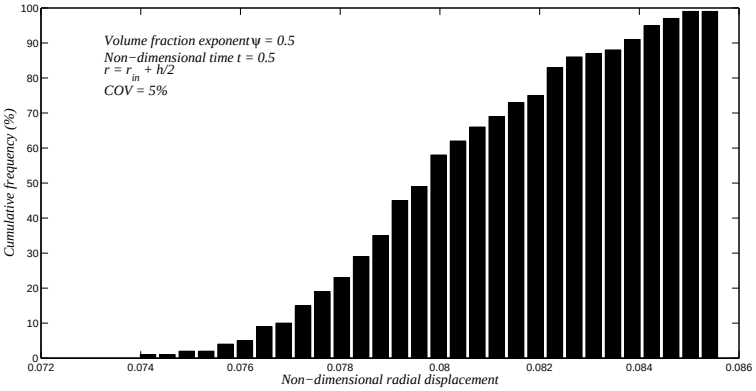

Figure 16: Cumulative frequency histogram of non-dimensional radial displacement for "$r = r_{in} + h/2$", "$\psi = 0.5$", "$\bar{t} = 0.5$" and "$COV = 5\%$".

gations corresponding to the maximum and minimum values of temperature can be tracked for some time instants in Fig.12 with $COV = 5\%$ and $\psi = 0.5$. The influence of various grading patterns in FGM on the thermal wave propagation corresponding to the maximum values of non-dimensional temperature is demonstrated in Fig.13 for $COV = 5\%$ and $\bar{t} = 0.25$.

The same behavior can be observed for the non-dimensional radial displacement

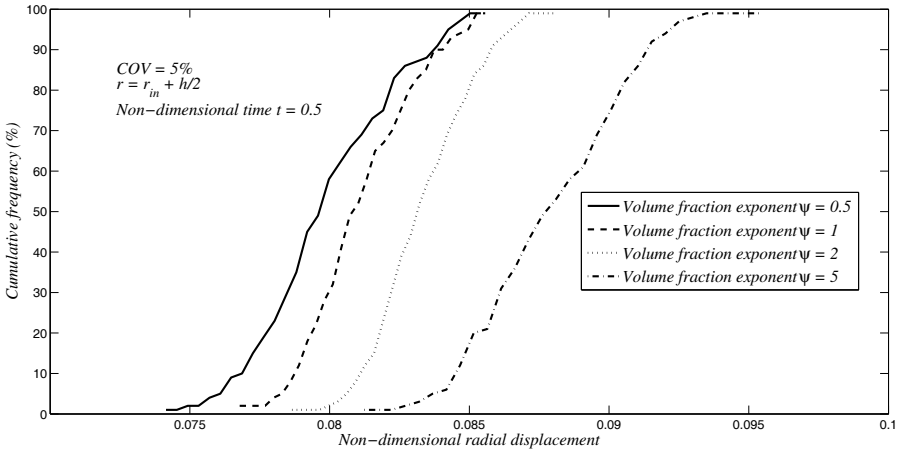

Figure 17: Cumulative distribution function (CDF) of non-dimensional temperature for various grading patterns in FGM and "$r = r_{in} + h/2$", "$COV = 5\%$", "$\bar{t} = 0.5$".

field in the coupled thermo-elasticity analysis for the FG thick hollow cylinder. Figs.14 to 17 show the behavior of statistical characteristics such as frequency histogram and cumulative distribution functions for the non-dimensional radial displacement with the same description and interpretation being valid as discussed for the temperature field. For example, with increasing the value of the volume fraction exponent, the CDF of the non-dimensional radial displacement is stretching in the displacement domain, as can be seen from Fig.17.

The effects of variation in value of COV on CDF of the non-dimensional radial displacement can be found in Fig.18 for $r = r_{in} + h/2$, $\psi = 0.5$ and $\bar{t} = 0.5$. Also, the time history of maximum, mean and minimum values of the non-dimensional radial displacement at the middle point of the thickness are presented in Fig.19 for $\psi = 0.5$ and $COV = 5\%$ with confirming the same behavior as for the temperature field.

It is shown in Fig.20 that the period of time history is affected by variation of the volume fraction exponent. The period of time oscillations for the non-dimensional radial displacement is decreased when the value of ψ is increased. Fig.21 shows the time history of maximum values of the non-dimensional radial displacement for various values of the COV at the middle point on the cylinder thickness for $\psi = 0.5$.

The distributions of the non-dimensional radial displacement along the thickness of

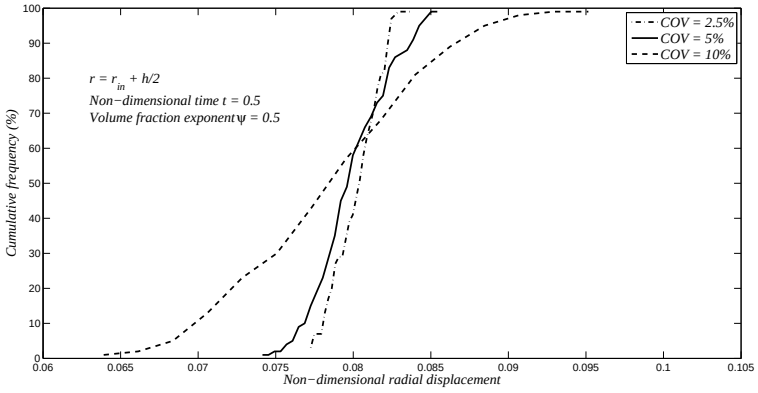

Figure 18: Cumulative distribution function (CDF) of non-dimensional radial displacement for various grading patterns in FGM and "$r = r_{in} + h/2$", "$\psi = 0.5$", "$\bar{t} = 0.5$".

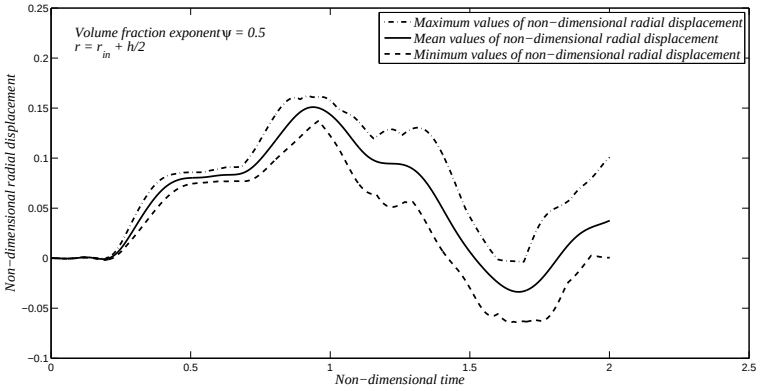

Figure 19: The time history of maximum, mean and minimum values of non-dimensional radial displacement for "$r = r_{in} + h/2$", "$\psi = 0.5$", "$\psi = 0.5$".

the FG thick hollow cylinder corresponding to the maximum, mean and minimum values of the non-dimensional radial displacement and various values of the COV can be observed in Figs. 22 and 23.

The behavior of the displacement field presented in Figs. 22 and 23 the behavior of the temperature field discussed earlier. Using the present method, the propagation

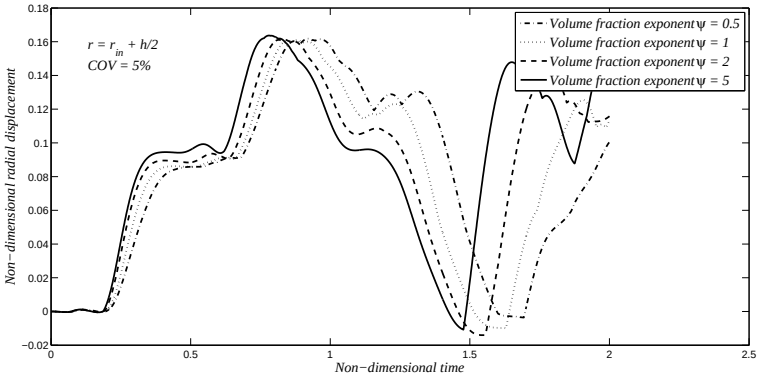

Figure 20: The time history of maximum values of non-dimensional radial displacement for various values of volume fraction exponent, "$r = r_{in} + h/2$" and "$COV = 5\%$".

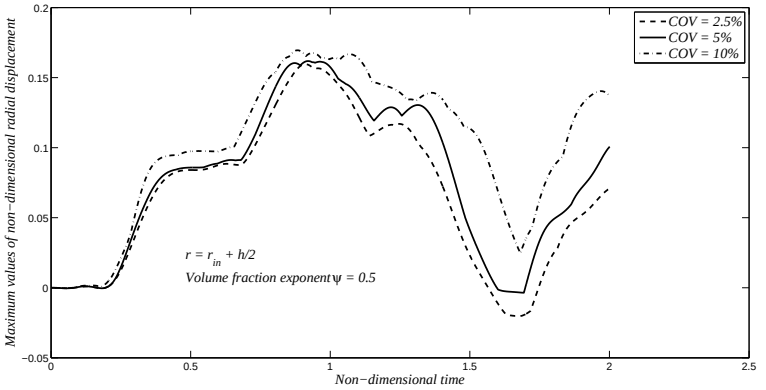

Figure 21: The time history of maximum values of non-dimensional radial displacement for various COV at middle point of thickness "$\psi = 0.5$".

of the radial displacement waves along the radial direction and corresponding to the maximum and minimum values of the non-dimensional radial displacement is revealed in Fig.24 at several time instants.

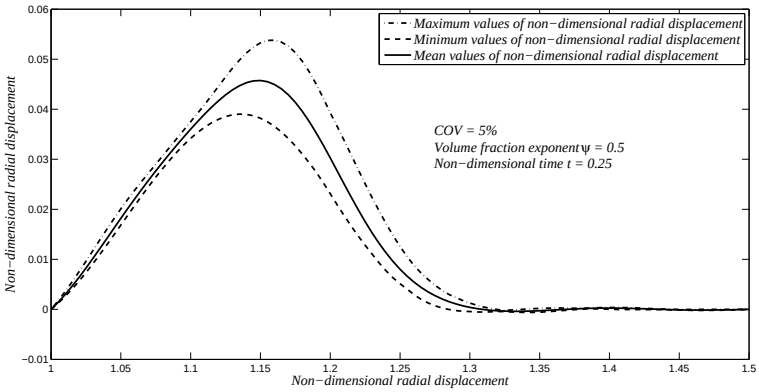

Figure 22: Non-dimensional radial displacement distribution across thickness of FG cylinder at "$\psi = 0.5$", "$\bar{t} = 0.25$" and "$COV = 5\%$".

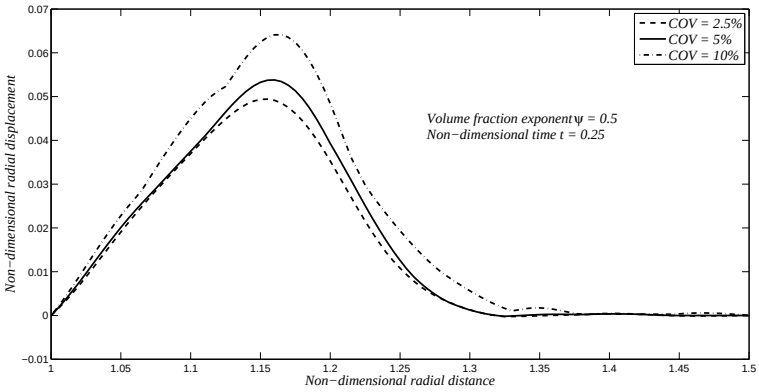

Figure 23: The distribution of maximum values of non-dimensional radial displacement across thickness of FG cylinder at "$\bar{t} = 0.25$" and "$\psi = 0.5$" and various COV.

5 Conclusion

The stochastic transient analysis of thermo-elastic wave propagation and time evolution of temperature and displacement fields based on Green-Naghdi theory of coupled thermo-elasticity (without energy dissipation) in a FG thick hollow cylinder are studied by developing the stochastic meshless local Petrov-Galerkin (MLPG) method. The presented method is based on the combination of the MLPG, the New-

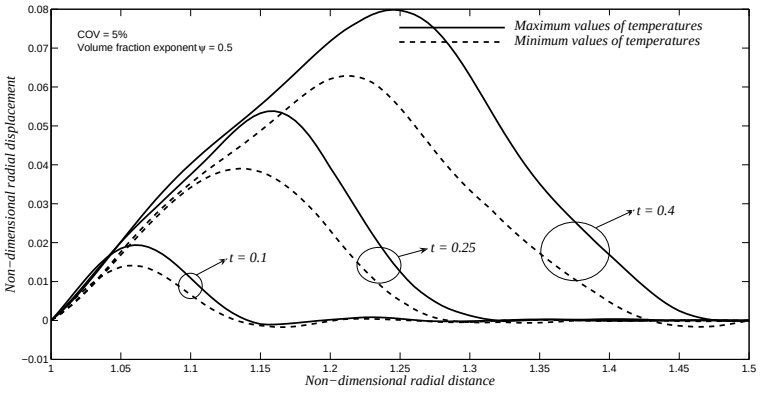

Figure 24: The propagation of radial displacement wave based on maximum and minimum values through radial direction for "$COV = 5\%$" and "$\psi = 0.5$".

mark finite difference (for discretization of time domain) methods and the Monte Carlo simulation (to generate the random variables). The constitutive material properties of FGM are considered to be random variables with the Gaussian distribution. Moreover, the material properties of FGM are assumed to vary along the radial direction as nonlinear function in terms of the volume fraction. The local integral equations are derived from the weak form of the governing equations with considering Heaviside step function as the test functions. The spatial variation of the temperature and radial displacement are approximated using an interpolation based on multiquadric radial basis function.

The thermo-elastic wave propagation corresponding to maximum values of both temperature and radial displacement fields are obtained for various grading patterns in FGM and for several values of coefficients of variations (COVs). The frequency histogram, cumulative frequency histogram and cumulative distribution function (CDF) of the temperature and displacement fields have been found for various grading patterns of FGM. The numerical results show that designers should consider the maximum values of the temperature and radial displacement fields in designing procedure in order to get a safe and reliable design of the FG cylinder subjected to thermal shock loadings. Furthermore, the effects of uncertainty in material properties of FGM on dynamic responses and wave propagation are studied in details and related statistical parameters are calculated using the presented method. In this approach, there is no need to consider the FG cylinder as a multi-layer cylinder with various material properties in each sub-cylinder. The present stochastic

MLPG method is very convenient computational method for stochastic analyses of structures made of FGMs with considering uncertainty in material properties. The MLPG method can be also applied to analyze the coupled thermo-elasticity problems based on other theories such as classical, the LS (Lord-Shulman) and the GL (Green-Linsay) theories in FG structures with uncertainty.

Acknowledgement: The authors (J.S. and V.S.) acknowledge the support by the Slovak Science and Technology Assistance Agency registered under numbers APVV-0032-10, APVV-0014-10 and the Slovak Grant Agency VEGA-2/0039/09.

References

Atluri, S.N. (2004): *The meshless method (MLPG) for domain & BIE discretization*. Tech. Science Press.

Chakraborty, A.; Rahman, S. (2008): Stochastic multiscale models for fracture analysis of functionally graded materials. *Engineering Fracture Mechanics*, vol. 75, pp. 2062–2086.

Chiba, R. (2009): Stochastic heat conduction analysis of a functionally graded annular disc with spatially random heat transfer coefficients. *Applied Mathematical Modelling*, vol. 33, pp. 507–523.

Chiba, R.; Sugano, Y. (2007): Stochastic thermoelastic problem of a functionally graded plate under random temperature load. *Arch. Appl. Mech.*, vol. 77, pp. 215–227.

Chiba, R. (2009): Stochastic thermal stresses in an FGM annular disc of variable thickness with spatially random heat transfer coefficients. *Meccanica*, vol. 44, pp. 159-176.

Chiba, R.; Sugano, Y. (2008): Stochastic analysis of a thermoelastic problem in functionally graded plates with uncertain material properties. *Arch. Appl. Mech.*, vol. 78, pp. 749–764.

Ferrante, F.J.; Graham-Brady, L.L. (2005): Stochastic simulation of non-Gaussian / non-stationary properties in a functionally graded plate. *Comput. Methods Appl. Mech. Eng.*, vol. 194, pp. 1675-1692.

Green, A.E.; Naghdi, P.M. (1993): Thermo-elasticity without energy dissipation. *Journal of Elasticity*, vol. 31, pp. 189-208.

Hosseini, S.M.; Shahabian, F. (2010): Reliability of Stress Field in Al-Al_2O_3 Functionally Graded Thick Hollow Cylinder subjected to Sudden Unloading, Considering Uncertain Mechanical Properties. *Materials and Design*, vol. 31, pp. 3748–3760.

Hosseini, S.M.; Sladek, J.; Sladek, V. (2011): Meshless local Petrov-Galerkin method for coupled thermo-elasticity analysis of a functionally graded thick hollow cylinder. *Eng. Anal. Bound. Elem.*, doi:10.1016/j.enganabound.2011.02.001.

Kitipornchai, S.; Yang, J.; Liew, K.M. (2006): Random vibration of the functionally graded laminates in thermal environments. *Comput. Methods Appl. Mech. Engrg.*, vol. 195, pp.1075–1095.

Rahman, S.; Chakraborty, A. (2007): A stochastic micromechanical model for elastic properties of functionally graded materials. *Mechanics of Materials*, vol. 39, pp. 548–563.

Saleh, M.M.; El-Kalla, I.L.; Ehab, M.M. (2007): Stochastic Finite Element Technique for Stochastic One-Dimension Time-Dependent Differential Equations with Random Coefficients. *Differential Equations and Nonlinear Mechanics*, Article ID 48527, pp. 1-16.

Shaker, A.; Abdelrahman, W.; Tawfik, M.; Sadek, E. (2008): Stochastic Finite element analysis of the free vibration of functionally graded material plates. *Computational Mechanics*, vol. 41, pp. 707–714.

Shahabian, F.; Hosseini, S.M. (2010): Stochastic dynamic analysis of a functionally graded thick hollow cylinder with uncertain material properties subjected to shock loading. *Materials and Design*, vol. 31, pp. 894-901.

Sladek, J.; Sladek, V.; Van Keer, R. (2003a): Meshless local boundary integral equation method for 2D elastodynamic problems. *Int. J. Num. Meth. Engn.*, vol.57, pp. 235-249.

Sladek, J.; Sladek, V.; Zhang, Ch. (2003b): Application of meshless local Petrov-Galerkin (MLPG) method to elastodynamic problems in continuously nonhomogeneous solids. *CMES: Computer Modeling in Engineering & Sciences,* vol. 4, pp. 637-648.

Sladek, J.; Sladek, V.; Zhang, Ch. (2003c): Transient heat conduction analysis in functionally graded materials by the meshless local boundary integral equation method. *Computational Material Science*, vol. 28, pp. 494-504.

Sladek, J.; Sladek, V.; Krivacek, J.; Zhang, Ch. (2003d): Local BIEM for transient heat conduction analysis in 3-D axisymmetric functionally graded solids. *Comput. Mech.*, vol. 32, pp.169-176.

Sladek, J.; Sladek, V.; Hon, Y.C. (2005): Inverse heat conduction problems by meshless local Petrov–Galerkin method. *Eng. Anal. Bound. Elem.*, vol. 30, pp. 650-661.

Sladek, J.; Sladek, V.; Atluri, S.N. (2001): A pure contour formulation for the meshless local boundary integral equation method in thermo-elasticity. *CMES:*

Computer Modeling in Engineering & Sciences, vol. 2, pp. 423-434.

Sladek J., Sladek V., Zhang Ch., Tan C.L. (2006): Meshless local Petrov-Galerkin method for linear coupled thermoelastic analysis. *CMES: Computer Modeling in Engineering & Sciences* 16, 57-68.

Sladek, J.; Sladek, V.; Tan, C.L.; Atluri, S.N. (2008a): Analysis of Transient Heat Conduction in 3D Anisotropic Functionally Graded Solids, by the MLPG Method. *CMES: Computer Modeling in Engineering & Sciences*, vol. 32, no. 3, pp. 161-174.

Sladek, V; Sladek, J; Zhang Ch. (2008b): Local integral equation formulation for axially symmetric problems involving elastic FGM. *Eng Anal Bound Elem*., vol. 32, pp. 1012-1024.

Taheri, H.; Fariborz, S.; Eslami, M.R. (2005): Thermoelastic analysis of an annulus using the Green-Naghdi model. *Journal of Thermal Stresses*, vol. 28, no. 9, pp. 911-927.

Yang, J.; Liew, K.M.; Kitipornchai, S. (2005a): Second-order statistics of the elastic buckling of functionally graded rectangular plates. *Composites Science and Technology*, vol. 65, pp. 1165–1175.

Yang, J.; Liew, K.M.; Kitipornchai, S. (2005b): Stochastic analysis of compositionally graded plates with system randomness under static loading. *International Journal of Mechanical Sciences*, vol. 47, pp. 1519–1541.